Journal of The Electrochemical Society, **154** (10) C558-C561 (2007)
0013-4651/2007/154(10)/C558/4/$20.00 © The Electrochemical Society

Modification of Trap Distributions in Anodic Aluminum Tunnel Barriers

Achim Walter Hassel[a,*,z] **and Detlef Diesing**[b]

[a]*Max-Planck-Institut für Eisenforschung GmbH, D-40237 Düsseldorf, Germany*
[b]*Fachbereich Chemie and Centre for Nanointegration, Universität Duisburg-Essen, D-45117 Essen, Germany*

The trap distribution in thin (d = 4.3 nm) aluminum oxide films was modified electrochemically and subsequently quantified in a solid-state device. A combined potentiodynamic/potentiostatic experiment enabled preparation of samples showing different trap distributions with negligible thickness variation. Potentiodynamic oxide formation at a scan rate of 100 mV s^{-1} was used to form the anodic oxide with many defects. Subsequent potentiostatic polarization allowed a systematic reduction of the number of defects by electromigrative annealing. These oxides were used as a dielectric barrier in a metal-insulator-metal multilayer system with a silver top electrode. The current response of these samples to voltage pulses was investigated over a wide range in current (100 nA–1 A) and time (1 μs–100 s). A separation of Debye charging, dielectric relaxation, and steady-state tunnel current was possible in the time domain. The dielectric relaxation showed a very strong dependence on the previous electromigrative annealing time being approximately 85 times higher for a short annealing time of 0.2 s as compared to the longest annealing time of 100 s. The steady-state tunnel current displayed a much weaker dependence of only a factor of 1.6 and changed mainly during the initial annealing step from 0.2 s to 1 s. In this way it is possible to prepare anodic oxide films of constant film thickness with variable trap site densities. These films have identical tunneling properties but display extremely different relaxation behaviors.
 [DOI: 10.1149/1.2766646]

Manuscript submitted April 21, 2007; revised manuscript received June 1, 2007. Available electronically August 8, 2007.

The steady-state corrosion current for homogeneous corrosion in aluminum/aluminum oxide/electrolyte systems is known to depend on several parameters such as temperature, pH, and composition of the electrolyte. The direct measurement of the corrosion current provides information only on the overall process and its dependence on the corrosion conditions. Conclusions on how the transport of charge and matter through these dense, highly insulating oxides proceeds cannot be drawn in a simple way. This requires methods with a significant deviation from the equilibrium conditions, ideally during oxide formation itself.

The oxide formation on valve metals such as Al, Hf, Nb, Ta, Ti, and Zr is generally described by the Cabrera–Mott model,[1-4] which describes a thermally activated hopping mechanism for the ionic transport in the oxide. This high-field model was extended by Lohrengel, taking into account the retardation that results from the space charge forming in the thin oxide film after injection of mobile ions from the interfaces.[5] A general problem during this investigation is the separation of the underlying processes such as Debye charging, dielectric relaxation, charge carrier injection, oxide growth, oxygen evolution, electron-transfer reactions, direct elastic tunneling, resonance tunneling, and corrosion.[6] To a limited extent such a separation is possible in the frequency domain in which different processes can be observed at distinct frequencies.[7] However, these investigations are usually performed under low-field conditions. High-field conditions enable additional processes such as bulk oxide formation,[8] formation of porous oxides,[9-12] anodic breakdown,[13-15] cathodic breakdown,[16,17] and spark anodizing.[18-20] Even electronic processes such as electronic tunneling[21,22] may alter dramatically, e.g., when the trapezoidal tunnel barrier changes into a triangle one under Fowler–Nordheim tunneling.[23]

The subsequent evaporation of a noble metal film such as silver, gold, or platinum onto the anodically formed oxide yields a solid-state device. This allows a detailed investigation in the absence of an oxygen source, and due to the absence of water, in a much wider temperature range. It was shown for a number of valve metals, such as Al, Hf, Nb, Ta, Ti, and Zr, that the breakdown fieldstrength of a metal-insulator-metal (MIM) layer system is identical to the electrochemical oxide formation field strength under potentiostatic conditions.[24] It is possible to overcome this limitation by a controlled, nonavalanching breakdown process[25] demonstrating the remaining mobility of the defects.

It is desirable to control the defects in the anodic oxide by the anodizing process. One possibility is a galvanostatic oxide formation; the field strength could be calculated from the ratio between final potential and film thickness. However, transient effects cannot be considered. More elegant is the control via scan rate during potentiodynamic oxide formation.[26] In principle it would be possible to choose potentiostatic conditions in electrolytes of different aggressivity, but this usually results in a nonhomogenous attack with a rough or porous surface.[9-12,27] In this work the preparation of samples with various trap concentrations is therefore realized by a potentiodynamic oxide formation with subsequent potentiostatic annealing. Separation of the underlying transport processes was realized in the time domain by high-resolution current transients of potentiostatic pulse experiments.

Experimental

All solutions were prepared from p.a. chemicals and deionized water (Millipore Q). An acetate buffer of pH 6.0 was used for the anodic oxidation. Thin aluminum metal films were evaporated onto a chemically cleaned microscopic slide from highly pure aluminum wires (99.999%) in a ultrahigh-vacuum (UHV) chamber with a Riber system (with a turbomolecular pump, an ion getter, and a cryopump). The base pressure was 1×10^{-6} Pa and was always better than 1×10^{-5} Pa during metal evaporation.[7]

Anodic oxidation was done by means of a scanning droplet cell.[28,29] This system prevents the delamination of metal films, localizes the electrochemical reaction to the intended area, and guarantees full potential control due to the true three-electrode arrangement that makes use of a microreference electrode.[30,31] A detailed description of the anodization procedure is given in the next section.

The samples were thoroughly rinsed with water to remove residues of the electrolyte and dried in a nitrogen stream. Finally, the silver top electrode (20 nm) was deposited in the above-mentioned UHV system.

All potentials in the electrolyte given here refer to the hydrogen electrode in the same solution (HESS).

Details of the electronic equipment that is capable of measuring current transients over 9 dec in time (1 μs to 1000 s) and more than 10 dec in current (1 A to 10 pA) are given elsewhere.[25]

* Electrochemical Society Active Member.
z E-mail: hassel@elchem.de

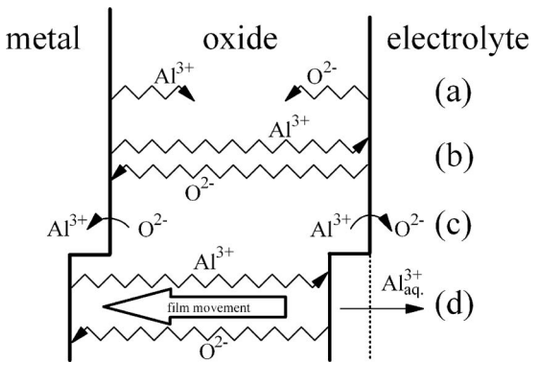

Figure 1. Schematic of an oxide-covered aluminum electrode in an electrolyte: (a) ion injection, (b) simultaneous flooding with anions and cations, (c) the start of replacement oxide growth, and (d) stationary corrosion condition. All arrows indicate transport of material except the thick, inward-directed arrow in section (d), which indicates the resulting inward movement of the oxide into the metal (see text for detailed discussion).

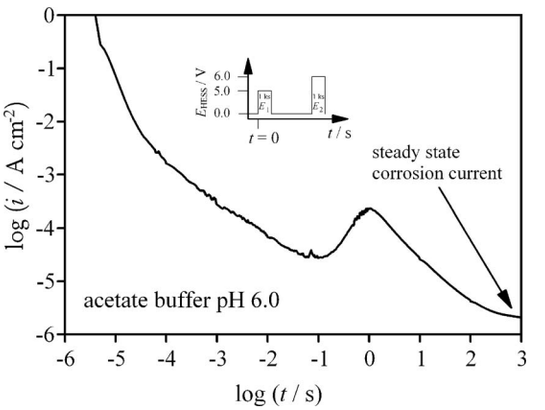

Figure 2. Current transient of potentiostatic oxide growth after a potential step from 0 to 6 V in pH 6.0 acetate buffer, applied to an oxide film that was initially grown at 5 V.

Results and Discussion

Figure 1 shows schematically the ionic processes in a thin oxide film during oxide growth. After increase of the field strength, metal cations are injected into the oxide from the metal/oxide interface and oxygen anions are injected from the electrolyte/oxide interface. This is indicated as process (a). In the electric field both ions simultaneously migrate through the oxide (b). Differences in size and charge of the ions influences their activation energy and thus, the resulting transport number. This transport number can be also influenced by the electric field strength, because the formation of a space-charge layer generally tends to equilibrate the transport contribution. After arrival at the opposite interface the mobile ions form new oxide at both interfaces together with their corresponding counterions. Because the oxide has a limited solubility in the adjacent electrolyte the corrosion cannot be neglected in this detailed observation. The corrosion rate might be very small, but it finally forms stationary corrosion conditions with the oxide reformation as the counterbalancing process. This is shown schematically as process (d). Because oxide corrosion takes place at the electrolyte interface only, but oxide formation under high-field conditions employs both the anionic and the cationic transport pathways, corrosion at constant film thickness results. These are the key conditions for achieving the lowest possible concentration of ions in the film. The field strength is still high at 0.625 GV m^{-1} in aluminum,[24] and the injection of ions from the interfaces is reduced to its minimum.

Figure 2 shows the current transient of a potentiostatic pulse experiment on aluminum in an acetate buffer of pH 6.0 at 25°C. The oxide was initially formed at 5 V vs HESS for 1000 s. The current transient shown here was recorded during a step to 6 V, as schematically shown in the inset. The transient is given in a double logarithmic plot with respect to the high dynamic in current and time which changes over six orders of magnitude in the first case and over nine orders for the latter. The Debye charging of the oxide dominates the current transient during the first 100 μs. The regime of a relaxation process follows, that was described by Jonscher,[32] and for the specific system given here by Rüße et al.[33] This specific behavior is utilized later to illuminate the differences in the film, resulting from the various formation conditions. After $\log(t/s) = -1$, i.e., after 100 ms, an increase in the current is observed that finds its maximum after 1 s. This maximum is commonly described as the beginning of oxide growth because from then on, the typical −1 slope of high-field oxide growth is observed. For longer polarization times the curve becomes flatter, corresponding to an increasing influence of the corrosion, that becomes dominant after about 10 ks. It is thus possible to separate the various processes in the time domain.

In this study, a modification of the concentration of mobile ions, which can also serve as traps for electronic processes, was achieved by a combined potentiodynamic formation process with subsequent electromigrative annealing. Figure 3 shows the current as a function of the potential during oxide formation on aluminum in a pH 6.0 acetate buffer. A scan rate of 100 mV s^{-1} was used for these experiments. The start potential was −0.5 V and a final potential of 1.1 V was chosen. The potential time diagram is schematically shown in the inset. The current is initially very small and suddenly increases when a potential of 0.2 V is exceeded. A maximum current of ca. 125 μA cm^2 is achieved prior to stabilization on the plateau level of 80 μA cm^2. After reaching the end potential of 1.1 V, the sample was held potentiostatically at this potential for time spans of 0.2, 1, 10, or 100 s. This is schematically shown in the inset of Fig. 4. The oxide thickness reached after potentiostatic oxide formation was coulometrically determined to be d = 4.3 nm.

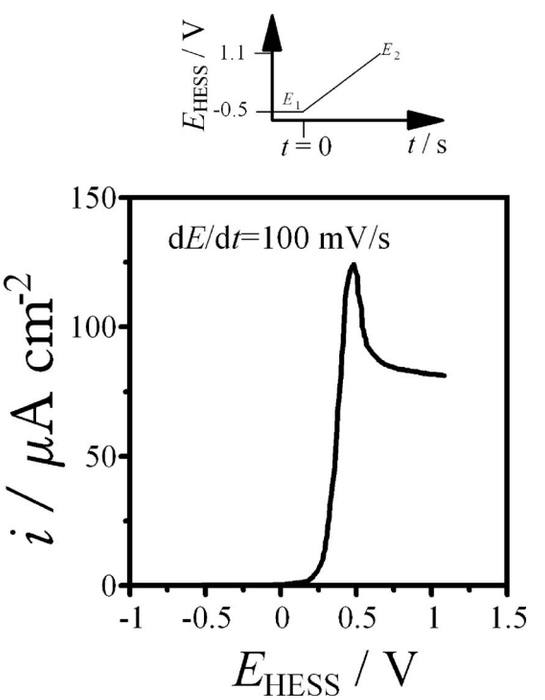

Figure 3. Procedure for varying the trap density, after potentiodynamic oxide formation.

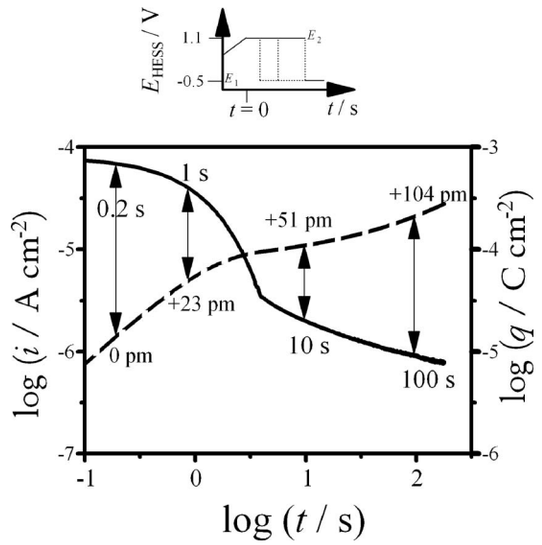

Figure 4. The potential is kept potentiostatically at the final oxide formation potential for various times to allow a definite depletion of the traps. The resulting charge transient is plotted vs the second *y* axis. Maximum possible film thickness (in picometers) increases are given as insets with respect to the value of 0.2 s potentiostatic polarization.

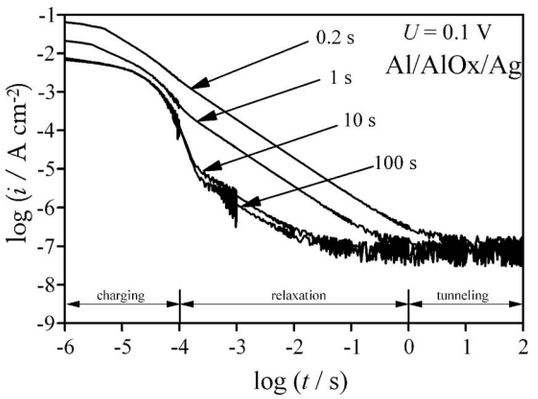

Figure 5. Current transients of the MIM system with differently prepared trap distributions (depletion time 0.2, 1, 10, 100 s) in the oxide.

The major step of trap modification is shown in Fig. 4. It displays a current transient of potentiostatic oxide formation recorded immediately after scanning the potential from −0.5 to 1.1 V. As in Fig. 2 a double logarithmic presentation was chosen with respect to the high dynamics of the system. Within 4 dec of time the current decreases by a factor of 100 and eventually falls below 1 μA cm^{-2}. The strongest change in the current is observed between 1 and 10 s. After 10 s the current becomes very flat, indicating that the underlying process is inhibiting itself more and more. A numerical integration of the current yields the charge transient that is plotted in the same graph. A charge of about 300 μC cm^{-2} is consumed after 100 s. The changes in the oxide thickness corresponding to the charge consumed were calculated assuming 100% current efficiency. The values are given in the figure and are illustrated by vertical arrows, ranging from 23 pm after 1 s over 51 pm after 10 s up to 104 pm after 100 s, always with respect to the shortest potentiostatic polarization of 0.2 s. The so-calculated thickness increase is an upper limit of the possible thickness increase but is probably smaller. Looking at the highest possible increase of 0.104 nm with respect to the oxide thickness of 4.3 nm, a maximum change in the film thickness of 2.5% can be considered. This is a remarkably small value and should be kept in mind when discussing the observed effects.[34,35]

After evaporation of a thin silver top electrode on the differently prepared oxide films, the resulting MIM systems were prepared for their subsequent characterization. Figure 5 shows the current transients after a potentiostatic pulse from 0 to 0.1 V. This voltage is directly applied to the MIM system in its two-electrode configuration. As before, the current transients are presented in a double-logarithmic plot. The initial period of capacitive charging lasts some 100 μs and shows the typical shape. The intermediate region of the graph shows the most pronounced differences. There is a clear order of current density with the previous potentiostatic anodization time; the longer it was the lower is the current in the relaxation region, ranging from 100 μs to 1 s. After about 1 s the current stabilizes at a current density of about 100 nA cm^{-2}, this is the region in which the steady-state tunnel current dominates.

The data in Fig. 6 was extracted from the transients in Fig. 5. The relaxation current at t = 2 ms is plotted in Fig. 6 as a function of the depletion time, i.e., the potentiostatic annealing time. The values obtained on different samples are given and a solid line is drawn through the average values. The relaxation current shows a very strong dependence on the depletion time. By extending this preparation time from 0.2 to 1 s the current decreases from 320 to 95 μA cm^{-2}, which is a reduction by a factor of 3.5. This reduction factor and the reduction factor of this current as a function of the increased depletion time is given in the figure. There is a tremendous reduction of the relaxation current by a factor of 85.4.

The data in Fig. 7 was also extracted from the transients shown in Fig. 5. The current at the end of each curve is in the nA range and remains constant. This constant range between 10 and 100 s was averaged and finally plotted as a function of the depletion time in Fig. 7. For potentiostatic polarization times of 1 s or more, the steady-state tunnel current remains constant at around 75 nA cm^{-2}. This proves that the previously observed strong differences on the relaxation current are completely independent of the steady-state tunnel current. It further demonstrates that the combined procedure consisting of a potentiodynamic oxide formation with subsequent potentiostatic electromigrative annealing does not change the film thickness to a measurable degree. The tunnel current depends exponentially on the film thickness and is therefore a very sensitive measure. Moreover, this result demonstrates that the physical process responsible for the dielectric relaxation has no influence on the steady-state tunnel current in alumina films a few nanometers thick.

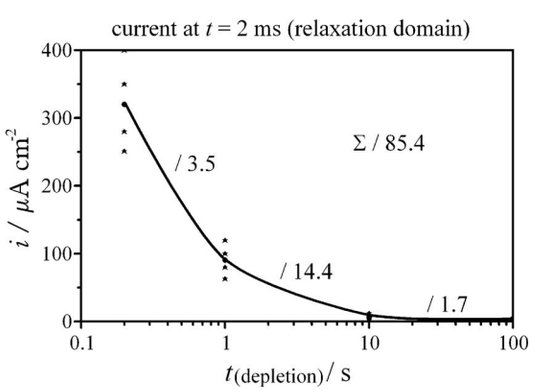

Figure 6. Comparison of the non-steady-state current at t = 2 ms for various depletion times as a function of the potentiostatic electric annealing time. (Data points from different samples are given as asterisks; mean values are given as solid dots connected with a curve).

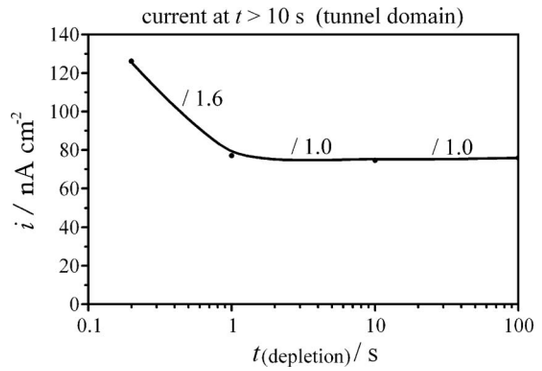

Figure 7. Comparison of steady-state current averaged between 10 and 100 s as a function the potentiostatic electric annealing time.

Conclusion

Thin anodic aluminum oxide films which were formed potentiodynamically were exposed to a certain field strength which depends on the electrolyte and the potential scan rate. The evaporation of a thin metal film that acted as top electrode allowed detailed electrical characterization of the films formed. The maximum field strength during anodization resulted in a defect concentration which influenced the dielectric behavior of the film in the MIM contact. It was shown that a subsequent potentiostatic polarization during oxide formation caused a continuous decrease of the number of defects. The influence of this additional polarization on the film thickness was negligible, which was proved by the fact that there was only a very minor influence on the steady-state tunnel current. This tunnel current is a very sensitive measure for the film thickness for alumina films produced in an acetate buffer due to the exponential dependence of the tunnel current from the barrier thickness. The duration of the potentiostatic polarization was varied and the fast decrease of the current showed that this electromigrative annealing was a self-inhibiting effect. It must be emphasized here that the properties of the resulting film depend on the thickness, the field strength, and the duration of field application.

The resulting dielectrics were electrically characterized in the time domain. By means of a special setup with sufficient resolution in current and time it became possible to follow the response of the MIM system to a potentiostatic pulse over 1000 s with a resolution of 1 μs. The current drops from the ampere range to a steady-state tunnel current in the 100 nA range. The strongest differences between the samples are found for the dielectric relaxation. There is a strict monotonic decrease of dielectric relaxation current with increasing annealing time during formation.

A higher current in the dielectric relaxation domain does not correlate with the subsequent tunnel current for alumina films produced in an acetate buffer. This means that the trap density does not have an influence on the tunneling process, pointing to a weak coupling between the tunnel and the relaxation processes. Hence, traps which could serve as intermediate states for resonance tunneling through the oxide obviously have only a negligible concentration in the tunneling path.

Acknowledgment

This work was supported by the DFG under the framework of SFB 616 Project A3.

The Max-Planck-Institut für Eisenforschung GmbH assisted in meeting the publication costs of this article.

References

1. N. Cabrera, *Philos. Mag.*, **40**, 175 (1949).
2. N. Cabrera and N. F. Mott, *Rep. Prog. Phys.*, **12**, 163 (1949).
3. A. Güntherschulze and H. Betz, *Z. Phys.*, **92**, 367 (1934).
4. A. Güntherschulze and H. Betz, *Z. Elektrochem. Angew. Phys. Chem.*, **37**, 726 (1931).
5. M. M. Lohrengel, *Mater. Sci. Eng., R.*, **11**, 243 (1993).
6. J. W. Schultze and A. W. Hassel, *Encyclopedia of Electrochemistry*, A. J. Bard and M. Stratmann, Editors, Vol. 4, *Corrosion and Oxide Films*, M. Stratmann and G. S. Frankel, Editors, S. 216–270 and 188–189, Wiley-VCH, Weinheim (2003).
7. D. Diesing, A. W. Hassel, and M. M. Lohrengel, *Thin Solid Films*, **342**, 282 (1999).
8. S. Gudic, J. Radosevic, and M. Kliskic, *J. Appl. Electrochem.*, **26**, 1027 (1996).
9. T. P. Hoar and N. F. Mott, *J. Phys. Chem. Solids*, **9**, 97 (1959).
10. K. Shimizu, K. Kobayashi, G. E. Thompson, and G. C. Wood, *Philos. Mag. A*, **66**, 643 (1992).
11. H. Masuda and K. Fukuda, *Science*, **268**, 1466 (1995).
12. A. Mozalev, A. Poznyak, I. Mozaleva, and A. W. Hassel, *Electrochem. Commun.*, **3**, 299 (2001).
13. V. K. Agarwal, *Thin Solid Films*, **24**, 55 (1974).
14. T. H. Distefano and M. Schatzkes, *J. Vac. Sci. Technol.*, **13**, 50 (1976).
15. S. Ikonopisov, *Electrochim. Acta*, **22**, 1077 (1977).
16. V. Parkhutik, J. M. Albella, and J. M. Martinez Duart, in *Modern Aspects of Electrochemistry*, Vol. 23, B. E. Conway, Editor, p. 315ff, Plenum Press, New York (1992).
17. A. W. Hassel and M. M. Lohrengel, *Electrochim. Acta*, **40**, 433 (1995).
18. K. H. Dittrich, W. Krysmann, P. Kurze, and H. G. Schneider, *Cryst. Res. Technol.*, **19**, 93 (1984).
19. F. Monfort, A. Berkani, E. Matykina, P. Skeldon, G. E. Thompson, H. Habazaki, and K. Shimizu, *Corros. Sci.*, **49**, 672 (2007).
20. J. Kawakita, M. Stratmann, and A. W. Hassel, *J. Electrochem. Soc.*, **154**, C294 (2007).
21. J. G. Simmons and G. W. Taylor, *Phys. Rev. B*, **5**, 553 (1972).
22. J. W. Schultze and V. A. Macagno, *Electrochim. Acta*, **31**, 355 (1986).
23. R. H. Fowler and L. Nordheim, *Proc. R. Soc. London, Ser. A*, **119**, 173 (1928).
24. A. W. Hassel and D. Diesing, *Thin Solid Films*, **414**, 296 (2002).
25. A. W. Hassel and D. Diesing, *Electrochem. Commun.*, **4**, 1 (2002).
26. C. G. Dunn, *J. Electrochem. Soc.*, **115**, 219 (1968).
27. H. Wu and K. R. Hebert, *Electrochim. Acta*, **47**, 1373 (2002).
28. A. W. Hassel and M. M. Lohrengel, *Electrochim. Acta*, **42**, 3327 (1997).
29. K. A. Lill, A. W. Hassel, G. Frommeyer, and M. Stratmann, *Electrochim. Acta*, **51**, 978 (2005).
30. A. W. Hassel, K. Fushimi, and M. Seo, *Electrochem. Commun.*, **1**, 180 (1999).
31. K. A. Lill and A. W. Hassel, *J. Solid State Electrochem.*, **10**, 941 (2006).
32. A. K. Jonscher, *Nature (London)*, **267**, 673 (1977).
33. S. Rüße, M. M. Lohrengel, and J. W. Schultze, *Solid State Ionics*, **72**, 29 (1994).
34. J. Schafer and C. J. Adkins, *J. Phys.: Condens. Matter*, **3**, 2907 (1991).
35. Y. Jeliazova, M. Kayser, B. Mildner, A. W. Hassel, and D. Diesing, *Thin Solid Films*, **500**, 330 (2006).